



# A New Approach for Designing Moving-Water Equilibria Preserving Schemes for the Shallow Water Equations

Yuanzhen Cheng<sup>1</sup> · Alina Chertock<sup>2</sup> · Michael Herty<sup>3</sup> · Alexander Kurganov<sup>1,4</sup> · Tong Wu<sup>1</sup>

Received: 24 October 2018 / Revised: 6 March 2019 / Accepted: 17 March 2019 /

Published online: 2 April 2019

© Springer Science+Business Media, LLC, part of Springer Nature 2019

## Abstract

We construct a new second-order moving-water equilibria preserving central-upwind scheme for the one-dimensional Saint-Venant system of shallow water equations. The idea is based on a reformulation of the source terms as integral in the flux function. Reconstruction of the flux variable yields then a third order equation that can be solved exactly. This procedure does not require any further modification of existing schemes. Several numerical tests are performed to verify the ability of the proposed scheme to accurately capture small perturbations of steady states.

**Keywords** Shallow water equations · Central-upwind scheme · Well-balanced method · Steady-state solutions (equilibria) · Moving-water and still-water equilibria

**Mathematics Subject Classification** 76M12 · 65M08 · 35L65 · 86-08 · 86A05

---

✉ Alexander Kurganov  
kurganov@math.tulane.edu

Yuanzhen Cheng  
ycheng5@tulane.edu

Alina Chertock  
chertock@math.ncsu.edu

Michael Herty  
herty@mathc.rwth-aachen.de

Tong Wu  
twu2@tulane.edu

<sup>1</sup> Mathematics Department, Tulane University, New Orleans, LA 70118, USA

<sup>2</sup> Department of Mathematics, North Carolina State University, Raleigh, NC 27695, USA

<sup>3</sup> Department of Mathematics, RWTH Aachen University, Templergraben 55, 52056 Aachen, Germany

<sup>4</sup> Department of Mathematics, Southern University of Science and Technology, Shenzhen 518055, China

### 1 Introduction

This paper is concerned with the Saint-Venant system of shallow water equations proposed in [16] and widely used to model water flows in rivers, canals, lakes, reservoirs and coastal areas. The equations for the water depth  $h(x, t) \geq 0$  and the velocity  $u(x, t)$  are given by

$$\begin{cases} h_t + q_x = 0, \\ q_t + \left(hu^2 + \frac{g}{2}h^2\right)_x = -ghB_x - g\frac{n^2}{h^{7/3}}|q|q. \end{cases} \tag{1.1}$$

Here,  $q(x, t) := h(x, t)u(x, t)$  is the discharge,  $B(x)$  is the bottom elevation,  $g$  is the constant gravitational acceleration, and  $n$  is the Manning friction coefficient.

The system (1.1) is a hyperbolic system of balance laws, which admits both smooth and nonsmooth solutions. A special class of the solutions are steady states at which the flux gradient in the second equation in (1.1) is exactly balanced by the geometric and friction source terms. Steady states are of great practical importance since many physically relevant solutions of (1.1) are, in fact, small perturbations of the steady states.

The steady-state solutions satisfy the time-independent system:

$$\begin{cases} q_x = 0, \\ \left(hu^2 + \frac{g}{2}h^2\right)_x = -ghB_x - g\frac{n^2}{h^{7/3}}|q|q. \end{cases} \tag{1.2}$$

In general, this system does not have an analytical solution. However, the “lake at rest” (*still-water*) equilibria form a class of particular steady states with the velocity of the water equal to zero:

$$q \equiv 0, \quad h + B \equiv \text{Const.}$$

For some particular (*moving-water*) ( $q \neq 0$ ) steady states, we refer the reader to [13] and references therein. If the bottom friction is neglected, that is, if  $n = 0$ , the general smooth moving-water equilibria are given by

$$q \equiv \text{Const}, \quad E := \frac{u^2}{2} + g(h + B) \equiv \text{Const}, \tag{1.3}$$

where  $E$  is the energy.

Capturing steady-state solutions or their small perturbations numerically is a challenging task as a straightforward implementation of shock capturing numerical methods typically leads to spurious oscillations unless a very fine computational grid is used. Indeed, if a scheme preserves the steady state up to the order of its formal accuracy, the spurious numerical waves may have larger magnitude than the water waves to be captured. Therefore, it is necessary to design well-balanced schemes, that is, schemes that are capable of exactly preserving steady-state solutions. We refer the reader to the non-exhaustive list of references on still-water equilibria preserving numerical methods [1,3,4,6,17,20,22,23,26,31,34,35]. The well-balanced property of these methods hinges on a special approximation of the geometric source term  $-ghB_x$ , which is relatively easy to construct. The case of the moving-water equilibria is substantially more complicated even in the frictionless case ( $n = 0$ ); see, e.g., [5,7,10,18, 22,33,36,37,41–43]. The difficulty is related to the fact that well-balanced approximations of the geometric source now need to include terms that are small for smooth solutions, but may become artificially large at discontinuities. In the nonzero friction case, only certain particular

moving-water equilibria could be exactly preserved by existing numerical methods; see, e.g., [9,13,22].

In this paper, we present a novel way of designing moving-water equilibria preserving schemes, which would not require a special approximation of the geometric or friction source terms. Following the idea from [11,15], we incorporate the source term in the discharge equation into its flux term and rewrite (1.1) in the following equivalent form:

$$\begin{cases} h_t + q_x = 0, \\ q_t + K_x = 0, \end{cases} \quad (1.4)$$

where

$$K := hu^2 + \frac{g}{2}h^2 + R, \quad (1.5)$$

so that  $K$  is a global equilibrium variable with

$$R(x, t) := g \int \left[ h(\xi, t) B_x(\xi) + \frac{n^2}{h^{7/3}(\xi, t)} |q(\xi, t)| q(\xi, t) \right] d\xi. \quad (1.6)$$

Indeed, the general (moving-water) steady state (which is a solution of (1.2)) can be expressed in terms of  $q$  and  $K$  as

$$q \equiv \text{Const}, \quad K \equiv \text{Const}. \quad (1.7)$$

The system (1.4) is a hyperbolic system with a global flux, which makes the development of an upwind scheme based on the solution of (generalized) Riemann problems difficult or even impossible. We therefore derive a Riemann-problem-solver-free central-upwind scheme, which can be quite easily applied to problems with global fluxes; see, e.g., [11,27]. Central-upwind schemes are Godunov-type finite-volume methods that were introduced in [29] and then further developed in [24,25,28,30]. Central-upwind schemes were also applied to the Saint-Venant system of shallow water equations. Still-water equilibria preserving central-upwind schemes were proposed in [23,26], while several moving-water equilibria preserving central-upwind scheme have been recently introduced in [10,13]. We also refer the reader to the recent review paper [22].

In this paper, we develop a moving-water equilibria preserving semi-discrete central-upwind scheme for the system (1.4). Like in every finite-volume method, the solution computed by the central-upwind scheme is realized in terms of the cell averages of  $h$  and  $q$ . When these quantities are available at a certain time level, we first follow the approach in [11,14,15,27] and obtain the discrete values of the equilibrium variable  $K$  using the midpoint quadrature for the spatial integral (1.5). Then, in order to derive a well-balanced scheme, we reconstruct the equilibrium variables  $q$  and  $K$  rather than conservative ones ( $h$  and  $q$ ), and use these reconstructed values to evaluate the numerical central-upwind fluxes. We enforce the positivity of the water depth  $h$  using the draining time-step technique from [4]; also see [3,10,15] (positivity-preserving property is another very important feature of numerical methods for the Saint-Venant system since if  $h$  is small, then even small numerical oscillations may lead to appearance of negative values of  $h$  and thus to a breakdown of numerical schemes since the eigenvalues of the Jacobian for the Saint-Venant system are  $u \pm \sqrt{gh}$ ).

The paper is organized as follows. A new moving-water equilibria preserving semi-discrete central-upwind scheme is derived in Sect. 2. The new scheme is tested on a variety of numerical examples in Sect. 3.

## 2 Semi-Discrete Central-Upwind Scheme

In this section, we describe a semi-discrete second-order central-upwind scheme for the Saint-Venant system (1.4). To this end, we rewrite (1.4) in the vector form in term of  $\mathbf{U} = (h, q)^T$  and  $\mathbf{F}(\mathbf{U}, B) = (q, K)^T$ :

$$\mathbf{U}_t + \mathbf{F}(\mathbf{U}, B)_x = 0. \tag{2.1}$$

We first discretize the spatial computational domain using finite-volume cells  $C_j = [x_{j-\frac{1}{2}}, x_{j+\frac{1}{2}}]$  of size  $\Delta x$  centered at  $x_j = j\Delta x$  with  $j = j_\ell, \dots, j_r$  and assume that the cell averages of the computed solution at a certain time level  $t$ ,

$$\bar{\mathbf{U}}_j(t) := \frac{1}{\Delta x} \int_{C_j} \mathbf{U}(x, t) \, dx,$$

are known. The semi-discrete central-upwind scheme for the system (2.1) reads as

$$\frac{d}{dt} \bar{\mathbf{U}}_j = - \frac{\mathbf{H}_{j+\frac{1}{2}} - \mathbf{H}_{j-\frac{1}{2}}}{\Delta x}, \tag{2.2}$$

where  $\mathbf{H}_{j+\frac{1}{2}}$  are the central-upwind numerical fluxes (see [23,26]):

$$\begin{aligned} \mathbf{H}_{j+\frac{1}{2}} &= \frac{a_{j+\frac{1}{2}}^+ \mathbf{F}(\mathbf{U}_{j+\frac{1}{2}}^-, B_{j+\frac{1}{2}}) - a_{j+\frac{1}{2}}^- \mathbf{F}(\mathbf{U}_{j+\frac{1}{2}}^+, B_{j+\frac{1}{2}})}{a_{j+\frac{1}{2}}^+ - a_{j+\frac{1}{2}}^-} \\ &\quad + \frac{a_{j+\frac{1}{2}}^+ a_{j+\frac{1}{2}}^-}{a_{j+\frac{1}{2}}^+ - a_{j+\frac{1}{2}}^-} (\mathbf{U}_{j+\frac{1}{2}}^+ - \mathbf{U}_{j+\frac{1}{2}}^-). \end{aligned} \tag{2.3}$$

Here,  $\mathbf{U}_{j+\frac{1}{2}}^\pm$  are left and right point values of  $\mathbf{U}$  at the cell interfaces  $x = x_{j+\frac{1}{2}}$ ,  $a_{j+\frac{1}{2}}^\pm$  are one-sided local speeds of propagation, and  $B_{j+\frac{1}{2}}$  are the point values of the continuous piecewise linear interpolant (see [26] for details), namely:

$$B_{j+\frac{1}{2}} := \frac{B(x_{j+\frac{1}{2}} + 0) + B(x_{j+\frac{1}{2}} - 0)}{2},$$

which reduces to  $B_{j+\frac{1}{2}} := B(x_{j+\frac{1}{2}})$  if  $B$  is continuous at  $x = x_{j+\frac{1}{2}}$ . In order to complete the construction of the well-balanced central-upwind scheme, we now need to evaluate  $\mathbf{U}_{j+\frac{1}{2}}^\pm$  and  $a_{j+\frac{1}{2}}^\pm$ .

We first describe a piecewise linear reconstruction procedure used to compute the point values  $\mathbf{U}_{j+\frac{1}{2}}^\pm = (h_{j+\frac{1}{2}}^\pm, q_{j+\frac{1}{2}}^\pm)$ . As it was shown in [23], a direct reconstruction of the conservative variables  $h$  and  $q$  would not lead to a well-balanced scheme. To overcome this difficulty, it was proposed in [23] to reconstruct the water surface  $w := h + B$  and discharge  $q$  variables, which results in a still-water equilibria preserving reconstruction. As mentioned in Sect. 1, the key point in designing a moving-water equilibria preserving scheme is to reconstruct the equilibrium variables  $\mathbf{V} := (q, K)$ , where  $K$  is defined in (1.5), to use the obtained reconstructions to evaluate  $\mathbf{V}_{j+\frac{1}{2}}^\pm = (q_{j+\frac{1}{2}}^\pm, K_{j+\frac{1}{2}}^\pm)$ , and then to recover the corresponding values  $h_{j+\frac{1}{2}}^\pm$  as explained below.

It should be observed that while the cell averages  $\bar{h}_j$  and  $\bar{q}_j$  are available, the values of  $K$  at the cell centers  $x = x_j$  are still to be computed. The latter can be done, for example, as follows. We approximate the global variable  $R$  defined in (1.6) using the midpoint rule:

$$R(x_{j+\frac{1}{2}}, t) \approx R_{j+\frac{1}{2}} := g \sum_{m=j_\ell}^j \left\{ \bar{h}_m (B_{m+\frac{1}{2}} - B_{m-\frac{1}{2}}) + \frac{n^2}{\bar{h}_m} |\bar{q}_m| \bar{q}_m \Delta x \right\}, \tag{2.4}$$

and then obtain the values of  $K$  at  $x = x_j$  as follows:

$$K_j = \frac{\bar{q}_j^2}{\bar{h}_j} + \frac{g}{2} \bar{h}_j^2 + \frac{R_{j+\frac{1}{2}} + R_{j-\frac{1}{2}}}{2}. \tag{2.5}$$

Note that formulae (2.4), (2.5) can be written in the following recursive way:

$$R_{j_\ell-\frac{1}{2}} = 0, \quad R_{j+\frac{1}{2}} = R_{j-\frac{1}{2}} + g \left[ \bar{h}_j (B_{j+\frac{1}{2}} - B_{j-\frac{1}{2}}) + \frac{n^2}{\bar{h}_j} |\bar{q}_j| \bar{q}_j \Delta x \right] \quad \text{for } j \geq j_\ell, \tag{2.6}$$

$$K_j = \frac{\bar{q}_j^2}{\bar{h}_j} + \frac{g}{2} \bar{h}_j^2 + R_{j-\frac{1}{2}} + \frac{g}{2} \left[ \bar{h}_j (B_{j+\frac{1}{2}} - B_{j-\frac{1}{2}}) + \frac{n^2}{\bar{h}_j} |\bar{q}_j| \bar{q}_j \Delta x \right]. \tag{2.7}$$

Given the values  $V_j := (\bar{q}_j, K_j)$ , a second-order piecewise linear reconstruction of  $V$  is constructed as

$$\tilde{V}(x) = V_j + (V_x)_j(x - x_j), \quad x \in C_j, \tag{2.8}$$

where  $(V_x)_j$  are at least first-order approximations of the corresponding derivatives  $V_x(x_j, t)$ . The non-oscillatory nature of the reconstruction (2.8) is ensured by applying a nonlinear limiter while computing the slopes there. In all of our numerical experiments, we have used a generalized minmod limiter (see, e.g., [32,38,39]):

$$(V_x)_j = \text{minmod} \left( \theta \frac{V_{j+1} - V_j}{\Delta x}, \frac{V_{j+1} - V_{j-1}}{2\Delta x}, \theta \frac{V_j - V_{j-1}}{\Delta x} \right), \quad \theta \in [1, 2],$$

where

$$\text{minmod}(z_1, z_2, \dots) := \begin{cases} \min(z_1, z_2, \dots), & \text{if } z_i > 0 \quad \forall i, \\ \max(z_1, z_2, \dots), & \text{if } z_i < 0 \quad \forall i, \\ 0, & \text{otherwise,} \end{cases}$$

and the parameter  $\theta$  is used to control the amount of the numerical dissipation—larger values of  $\theta$  correspond to a sharper reconstruction, but more dispersive reconstruction. The point values of  $V$  at the cell interface  $x = x_{j+\frac{1}{2}}$  are then computed as

$$V_{j+\frac{1}{2}}^- := \tilde{V}(x_{j+\frac{1}{2}} - 0) = V_j + \frac{\Delta x}{2} (V_x)_j, \\ V_{j+\frac{1}{2}}^+ := \tilde{V}(x_{j+\frac{1}{2}} + 0) = V_{j+1} - \frac{\Delta x}{2} (V_x)_{j+1}.$$

Equipped with  $q_{j+\frac{1}{2}}^\pm, K_{j+\frac{1}{2}}^\pm, R_{j+\frac{1}{2}}$ , the point values  $h_{j+\frac{1}{2}}^\pm$  can be obtained by solving the nonlinear algebraic equations, arising from the definition of the global variable  $K$  in (1.5):

$$\varphi(h) := \frac{(q_{j+\frac{1}{2}}^i)^2}{h} + \frac{g}{2}h^2 + R_{j+\frac{1}{2}} - K_{j+\frac{1}{2}}^i = 0, \quad i \in \{+, -\}. \tag{2.9}$$

Let us solve the equation in (2.9) for  $h_{j+\frac{1}{2}}^+$  (the solution for  $h_{j+\frac{1}{2}}^-$  is obtained in a similar manner). First, we note that one can easily show that the equation for  $h_{j+\frac{1}{2}}^+$  does not have any positive solutions unless

$$(q_{j+\frac{1}{2}}^+)^4 \leq \frac{8(K_{j+\frac{1}{2}}^+ - R_{j+\frac{1}{2}})^3}{27g}. \tag{2.10}$$

If (2.10) is not satisfied (which is a very unlikely case), we reconstruct  $\tilde{w}$  and set

$$h_{j+\frac{1}{2}}^+ = w_{j+\frac{1}{2}}^+ - B_{j+\frac{1}{2}}. \tag{2.11}$$

If (2.10) is satisfied, then there will be two possibilities. First, in the case  $q_{j+\frac{1}{2}}^+ = 0$ , we obtain the unique positive solution

$$h_{j+\frac{1}{2}}^+ = \sqrt{\frac{2(K_{j+\frac{1}{2}}^+ - R_{j+\frac{1}{2}})}{g}},$$

while if  $q_{j+\frac{1}{2}}^+ \neq 0$ , we solve the equation for  $h_{j+\frac{1}{2}}^+$  in (2.9) exactly and obtain the following three solutions:

$$h_{j+\frac{1}{2}}^+ = 2\sqrt{P} \cos\left(\frac{1}{3}[\Theta + 2\pi k]\right), \quad k = 0, 1, 2,$$

where

$$P := \frac{2(K_{j+\frac{1}{2}}^+ - R_{j+\frac{1}{2}})}{3g} \quad \text{and} \quad \Theta := \arccos\left(-\frac{(q_{j+\frac{1}{2}}^+)^2}{gP^{3/2}}\right).$$

One can show that one of these roots is negative, while the other two roots, which correspond to the subsonic and supersonic cases, are positive. We single out the physically relevant solution by choosing a root that is closer to the corresponding value of  $h_{j+\frac{1}{2}}^+$  given in (2.11).

**Remark 2.1** We notice that when  $h_{j+\frac{1}{2}}^+$  is computed using (2.11), it may be negative. In order to preserve the nonnegativity of reconstructed point values of  $h$ , we have implemented the positivity correction procedure proposed in [26, Sect. 2.2]

Finally, the one-sided local speeds of propagation  $a_{j+\frac{1}{2}}^\pm$  in (2.3) are estimated using the largest and smallest eigenvalues of the Jacobian  $\partial F/\partial \mathbf{U}$  and given by:

$$a_{j+\frac{1}{2}}^+ = \max\left\{u_{j+\frac{1}{2}}^- + \sqrt{gh_{j+\frac{1}{2}}^-}, u_{j+\frac{1}{2}}^+ + \sqrt{gh_{j+\frac{1}{2}}^+}, 0\right\},$$

$$a_{j+\frac{1}{2}}^- = \min\left\{u_{j+\frac{1}{2}}^- + \sqrt{gh_{j+\frac{1}{2}}^-}, u_{j+\frac{1}{2}}^+ + \sqrt{gh_{j+\frac{1}{2}}^+}, 0\right\}.$$

**Remark 2.2** It is easy to check that the designed semi-discrete second-order central-upwind scheme is capable of preserving discrete moving-water equilibria. Indeed, if one takes the steady-state data  $\bar{q}_j \equiv \hat{q}$ ,  $K_j \equiv \hat{K}$  and substitutes them into (2.2), (2.3), the right-hand side (RHS) of (2.2) will vanish since in this case, the numerical fluxes (2.3) are reduced to  $H_{j+\frac{1}{2}} \equiv (\hat{q}, \hat{K})$ .

**Remark 2.3** We would like to point out that in the frictionless case ( $n = 0$ ), the steady states (1.3) and (1.7) are equivalent for smooth solutions in the continuous setting. In the discrete setting, however, these steady states are different as the integral in (1.6) is computed using a quadrature, and thus the presented central-upwind scheme can preserve the moving-water equilibrium (1.7) only. In fact, the proposed scheme is capable of preserving a discrete version of the steady state (1.7), which is about  $\mathcal{O}((\Delta x)^2)$  away from the analytical one. Moreover, as no explicit formulae (in terms of the evolved quantities  $h$  and  $q$ ) of moving-water equilibria are available, it is our conjecture that no well-balanced scheme capable of exactly preserving the analytical moving-water steady states, can be developed.

**Remark 2.4** We note that in (almost) dry regions, the values  $h_{j+\frac{1}{2}}^\pm$  can be very small or even zero. This may not allow one to (accurately) compute the values of the velocity  $u_{j+\frac{1}{2}}^\pm$ , which may become artificially large. We therefore desingularize the velocity computation as follows:

$$u_{j+\frac{1}{2}}^\pm = \frac{2h_{j+\frac{1}{2}}^\pm q_{j+\frac{1}{2}}^\pm}{(h_{j+\frac{1}{2}}^\pm)^2 + \max\{(h_{j+\frac{1}{2}}^\pm)^2, \varepsilon^2\}}.$$

For consistency, the values  $q_{j+\frac{1}{2}}^\pm$  are then recomputed using  $q_{j+\frac{1}{2}}^\pm = h_{j+\frac{1}{2}}^\pm \cdot u_{j+\frac{1}{2}}^\pm$ . In all of our numerical experiments, we have taken  $\varepsilon = 10^{-8}$ . A similar desingularization technique has to be implemented whenever  $\bar{h}_j$  in the denominator in (2.5) is small. We note that one may use other desingularization strategies; see, e.g., the discussion in [22,26].

**Remark 2.5** Notice that the second component of the central-upwind flux (2.3) can be rewritten as

$$H_{j+\frac{1}{2}}^{(2)} = \widehat{H}_{j+\frac{1}{2}}^{(2)} + R_{j+\frac{1}{2}}, \tag{2.12}$$

where

$$\begin{aligned} \widehat{H}_{j+\frac{1}{2}}^{(2)} := & \frac{a_{j+\frac{1}{2}}^+ (K_{j+\frac{1}{2}}^- - R_{j+\frac{1}{2}}) - a_{j+\frac{1}{2}}^- (K_{j+\frac{1}{2}}^+ - R_{j+\frac{1}{2}})}{a_{j+\frac{1}{2}}^+ - a_{j+\frac{1}{2}}^-} \\ & + \frac{a_{j+\frac{1}{2}}^+ a_{j+\frac{1}{2}}^-}{a_{j+\frac{1}{2}}^+ - a_{j+\frac{1}{2}}^-} (q_{j+\frac{1}{2}}^+ - q_{j+\frac{1}{2}}^-). \end{aligned} \tag{2.13}$$

Substituting then (2.12) and (2.13) into the second component of the ODE system (2.2) and taking into account (2.6) results in

$$\frac{d}{dt} \bar{q}_j = -\frac{\widehat{H}_{j+\frac{1}{2}}^{(2)} - \widehat{H}_{j-\frac{1}{2}}^{(2)}}{\Delta x} - g \bar{h}_j \frac{B_{j+\frac{1}{2}} - B_{j-\frac{1}{2}}}{\Delta x} - g \frac{n^2}{\bar{h}_j^{7/3}} |\bar{q}_j| \bar{q}_j. \tag{2.14}$$

**Remark 2.6** The presented central-upwind semi-discretization results in the system of ODEs (2.2), which should be integrated in time by a sufficiently accurate, efficient and stable ODE solver. In all of our numerical experiments, we have used the second-order steady state and sign preserving semi-implicit Runge–Kutta SI-RK3 method developed in [12]. To this end, we have to replace the second equation in (2.2) with an equivalent ODE (2.14) so that the last term on the RHS of (2.14) can be treated in a semi-implicit manner as it was done in [12,13].

During the time evolution, the positivity of the computed values  $\bar{h}_j(t + \Delta t)$  is ensured using the “draining” time step technique proposed in [4]; we refer the reader to [10] for a detailed description.

### 3 Numerical Examples

We test the performance of the proposed semi-discrete second-order central-upwind scheme on numerical examples used in [10]. In these examples, we consider the cases of both continuous and discontinuous bottom topographies. In all of the examples, we use the following parameters: the gravitational constant  $g = 9.812$  (except for Example 3, where we take  $g = 9.81$ ), the computational domain  $[0, 25]$  if not stated otherwise; the minmod parameter  $\theta = 1.3$ ; and a CFL number of 0.5.

We also compare the results obtained by the proposed moving-water equilibria preserving central-upwind scheme (New Scheme) with the ones computed by the still-water equilibria preserving central-upwind scheme (Old Scheme) from [26].

#### 3.1 Frictionless Saint-Venant System ( $n = 0$ )

We first consider a frictionless case, for which a moving-water equilibria preserving central-upwind scheme has been recently derived in [10] based on the reconstruction of the equilibrium variables  $q$  and  $E$ . The New Scheme may be viewed as an alternative to the scheme from [10], and in this section we show how the New Scheme performs in the examples that were used in [10] (in fact, we have tested the New Scheme on all of the examples from [10] and draw a clear conclusion that in the frictionless case both central-upwind schemes lead to very similar numerical solutions).

**Example 1 Accuracy Test.** In this example, taken from [26,33], we check the experimental rate of convergence. The initial data and the bottom topography function are

$$h(x, 0) = 5 + e^{\cos(2\pi x)}, \quad q(x, 0) = \sin(\cos(2\pi x)), \quad B(x) = \sin^2(\pi x),$$

and the 1-periodic boundary conditions are imposed (the computational domain in this example is  $[0, 1]$ ). Since the exact solution is not known, we use a numerical solution computed on a very fine mesh with 51,200 uniform grid cells as a reference one. The solution at time  $t = 0.01$  is still smooth and we measure the  $L^1$ -errors for both  $h$  and  $q$ . The results are reported on Table 1, where one can clearly observe the experimental second order of accuracy as expected.

**Example 2 Convergence to Steady States.** In this example, we study the convergence in time towards steady flow over a bump where the bottom topography function is continuous and given by

**Table 1** Example 1:  $L^1$ -errors and experimental convergence rates

Number of grid cells	$h$		$q$	
	$L^1$ -error	Rate	$L^1$ -error	Rate
50	1.51e-03	–	1.21e-00	–
100	3.06e-04	2.30	2.26e-01	2.42
200	6.68e-05	2.20	4.90e-02	2.21
400	1.54e-05	2.12	1.17e-02	2.06
800	3.76e-06	2.04	2.95e-03	1.99
1600	9.29e-07	2.02	7.34e-04	2.01

$$B(x) = \begin{cases} 0.2 - 0.05(x - 10)^2, & \text{if } 8 \leq x \leq 12, \\ 0, & \text{otherwise.} \end{cases} \tag{3.1}$$

Depending on the initial and boundary conditions, the flow may be subcritical, supercritical or transcritical. We consider the following three sets of initial and boundary data (Cases (b)–(c) are taken from [19,40]; Case (a) is similar to a test problem considered in [21]):

(a) *Supercritical flow* with

$$\begin{aligned} h(x, 0) &= 2 - B(x), & q(x, 0) &\equiv 0, \\ h(0, t) &= 2, & q(0, t) &= 24; \end{aligned} \tag{3.2}$$

(b) *Subcritical flow* with

$$\begin{aligned} h(x, 0) &= 2 - B(x), & q(x, 0) &\equiv 0, \\ q(0, t) &= 4.42, & h(25, t) &= 2; \end{aligned} \tag{3.3}$$

(c) *Transcritical flow* with

$$\begin{aligned} h(x, 0) &= 0.33 - B(x), & q(x, 0) &\equiv 0, \\ q(0, t) &= 0.18, & h(25, t) &= 0.33. \end{aligned} \tag{3.4}$$

In all of these three cases, we compare the numerical solutions obtained by the New and Old Schemes at  $t = 500$  using 100 uniform grid cells. The obtained numerical results are shown in Figs. 1, 2 and 3. As one can see, the water depth  $h$  obtained by the New and Old Schemes are very close to the corresponding steady states in all three cases, while the equilibrium variables  $q$  and  $K$  are accurately computed only by the New Scheme and only in the smooth Cases (a) and (b). In Case (c), both the New and Old Schemes fail to accurately resolve the equilibria since the errors at the shock are  $\mathcal{O}(1)$  for both schemes (this result is expected since neither of the studied schemes preserves nonsmooth steady states). It should

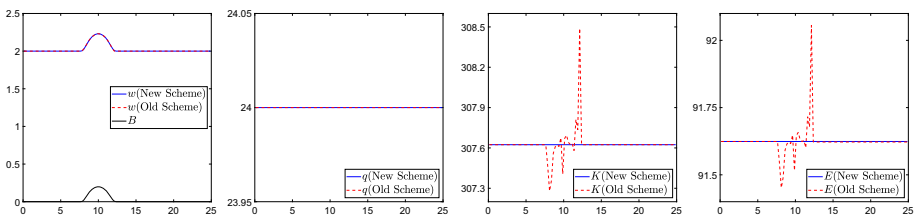


**Fig. 1** Example 2, Case (a):  $w, q, K$  and  $E$  (from left to right) computed by the New and Old Schemes

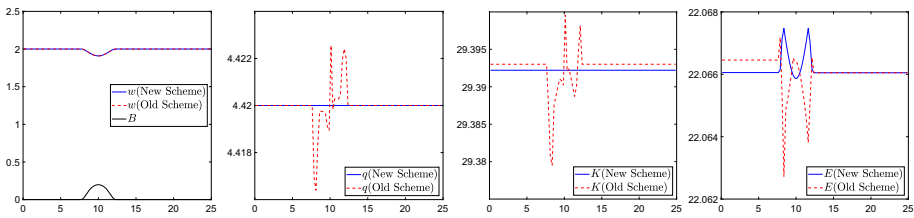


Fig. 2 Example 2, Case (b):  $w, q, K$  and  $E$  (from left to right) computed by the New and Old Schemes

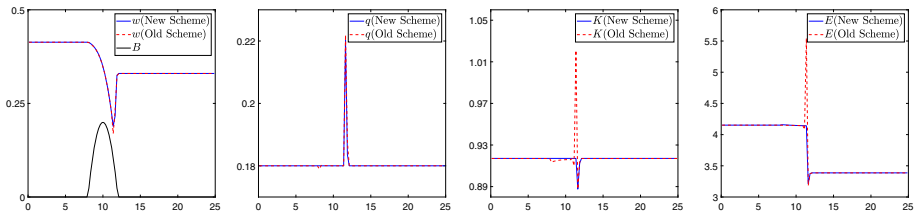


Fig. 3 Example 2, Case (c):  $w, q, K$  and  $E$  (from left to right) computed by the New and Old Schemes

be observed that for smooth solutions of the frictionless Saint-Venant system, the steady states (1.3) and (1.7) are equivalent and therefore in each one of the Figs. 1, 2 and 3 we also plot the computed values of  $E$ . We emphasize that for the New Scheme,  $E$  is not an equilibrium variable. However, in Case (a),  $E$  is still computed very accurately.

### 3.2 Saint-Venant System with Friction ( $n \neq 0$ )

We now test the proposed moving-water equilibria preserving central-upwind scheme in the presence of the Manning friction term. In Example 3, we take  $n = 0.03$ , while in Examples 4–8, we set  $n = 0.05$ .

**Example 3 Accuracy Test.** In this example taken from [2, 13], we consider a subcritical flow over a nonflat bottom. As described in [2, 13], the system (1.1) admits the steady-state solution with

$$h_{st}(x) = 0.8 + \frac{1}{4} \exp \left[ -\frac{135}{4} \left( \frac{x - 75}{150} \right)^2 \right], \quad q_{st}(x) \equiv 2,$$

and the bottom topography function  $B$  satisfying the following ODE:

$$B'(x) = \left( \frac{4}{9.81 h_{st}^3(x)} - 1 \right) h'_{st}(x) - \frac{0.0036}{h_{st}^{10/3}(x)},$$

which is numerically integrated on the fine mesh with 6400 uniformly distributed grid points.

We take the computational domain  $[0, 150]$  and implement the following boundary conditions by setting the ghost cell values to be

$$\bar{h}_{x_{\ell}-1} := 2\bar{h}_{j_{\ell}} - \bar{h}_{x_{\ell}+1}, \quad \bar{q}_{x_{\ell}-1} := 2, \quad \bar{h}_{j_r+1} := h_{st}(x_{j_r+1}), \quad \bar{q}_{j_r+1} := \bar{q}_{j_r}.$$

We test our scheme on different grids varying the number of cells from 50 to 400 and study the convergence rate by comparing the computed solutions with the steady-state one. As one can see, the designed method preserves  $q$  within (almost) the machine accuracy, while

**Table 2** Example 3: The  $L^1$ - and  $L^\infty$ -errors and convergence rates for  $h$  and  $q$

Number of grid cells	$h$				$q$	
	$L^1$ -error	Rate	$L^\infty$ -error	Rate	$L^1$ -error	$L^\infty$ -error
50	2.4676e-04	–	9.6741e-04	–	7.5007e-15	1.3767e-14
100	6.1545e-05	2.0034	2.4247e-04	1.9963	1.5852e-14	2.8644e-14
200	1.5385e-05	2.0001	6.0648e-05	1.9993	4.2926e-14	8.0824e-14
400	3.8458e-06	2.0002	1.5165e-05	1.9997	9.8251e-14	1.7963e-13

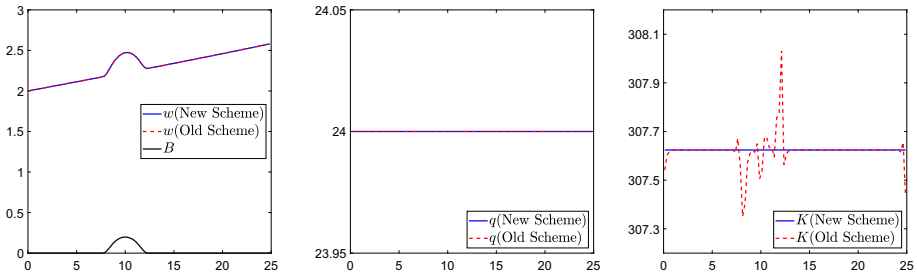


**Fig. 4** Example 4, Case (a):  $w$ ,  $q$  and  $K$  (from left to right) computed by the New and Old Schemes

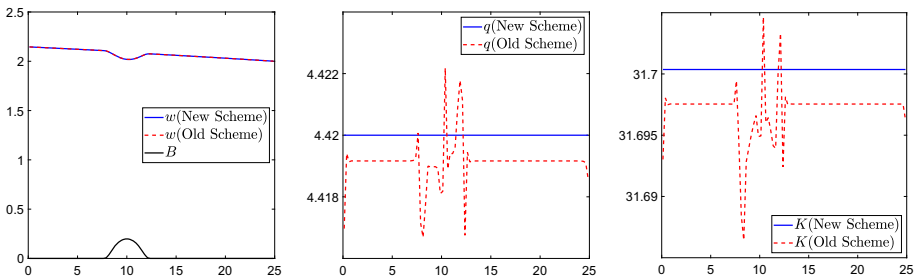


**Fig. 5** Example 4, Case (b):  $w$ ,  $q$  and  $K$  (from left to right) computed by the New and Old Schemes

$h$  is computed within the expected second order of convergence rate (due to the piecewise linear approximation of the bottom topography); see Table 2, where we show both the  $L^1$ - and  $L^\infty$ -norms of the errors together with the experimental convergence rates for  $h$ .

**Example 4 Convergence to Steady States (Continuous Bottom Topography).** This is a modification of Example 2 with the only difference that we now take into account the Manning friction term. We still consider the same three cases: super- [Case (a)], sub- [Case (b)] and transcritical [Case (c)] ones, but considering the same initial and boundary conditions as in (3.2), (3.3) and (3.4), respectively.

As in Example 2, we compare the numerical solutions obtained by the New and Old Schemes at  $t = 500$  using 100 uniform grid cells. The obtained numerical results are shown in Figs. 4, 5 and 6. One may notice that as in the frictionless case, the water depth  $h$  obtained by the New and Old Schemes are very close to the corresponding steady states in all of the three cases. One can also see that in Case (a), there is almost no difference in the computed values of  $q$ , while the second equilibrium variable  $K$  computed by the Old Scheme contains

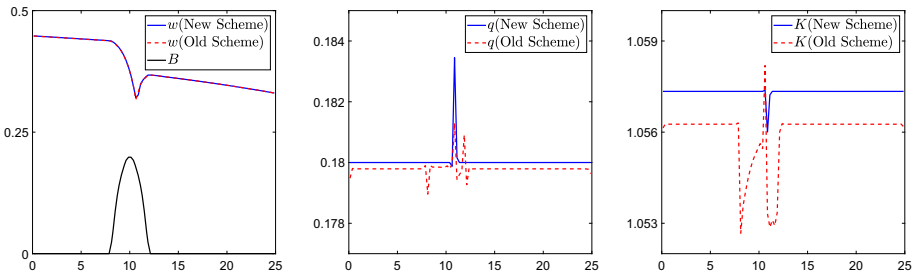


**Fig. 6** Example 4, Case (c):  $w$ ,  $q$  and  $K$  (from left to right) computed by the New and Old Schemes

visible oscillations. In Case (b), both  $q$  and  $K$  computed by the New Scheme are very accurate, while the Old Scheme results are not only oscillatory, but also seem to oscillate about an incorrect equilibrium. In Case (c), both the New and Old Schemes fail to accurately resolve the equilibria since the errors at the shock are  $\mathcal{O}(1)$  for both schemes. However, both  $q$  and  $K$  computed by the Old Scheme are shifted and contain significant oscillations in the smooth parts as well.

**Example 5 Small Perturbations of Moving-Water Equilibria (Continuous Bottom Topography).**

In this example, we test the performance of the New Scheme in the presence of small perturbations of the moving-water equilibria. We consider the continuous bottom topography function (3.1). The initial data are obtained by adding a small positive number 0.001 for  $x \in [4.5, 5.5]$  to the water depth for  $h$  obtained from the following two sets of the steady-state data:

(a) *Supercritical flow* with

$$q(x, 0) \equiv 24, \quad K(x, 0) \equiv 307.624; \tag{3.5}$$

(b) *Subcritical flow* with

$$q(x, 0) \equiv 4.42, \quad K(x, 0) \equiv 31.7005. \tag{3.6}$$

We note that the data in (3.5) and (3.6) are given in terms of  $q$  and  $K$  rather than in  $h$  and  $q$ . However, in order to start the computation at time  $t = 0$ , one needs to obtain the values of  $h_j$ . This can be done by solving the nonlinear equation (2.7), in which  $R_{j-\frac{1}{2}}$  are obtained from the recursive formula (2.6).

We first compute the numerical solutions using the New and Old Schemes until the final time  $t = 1$  with 100 uniform grid cells. In Figs. 7 and 8, we compare the difference between the obtained  $h$  and the background moving steady-state water depth. As one can see, the Old Scheme generates large spurious oscillations; see the dashed lines in Figs. 7 (left) and 8 (left). As we refine the mesh to 1000 uniform grid cells, the magnitude of the oscillations decreases as expected; see the solid lines in Figs. 7 (left) and 8 (left). On the other hand, the results obtained by the New Scheme are oscillation-free on both the coarse and fine meshes as one can clearly see in Figs. 7 (right) and 8 (right). This shows the advantage of the newly derived well-balanced scheme.

**Example 6 Convergence to Steady States (Discontinuous Bottom Topography).** In this example, we study the convergence in time towards a steady flow over a bump with the discontinuous bottom topography function

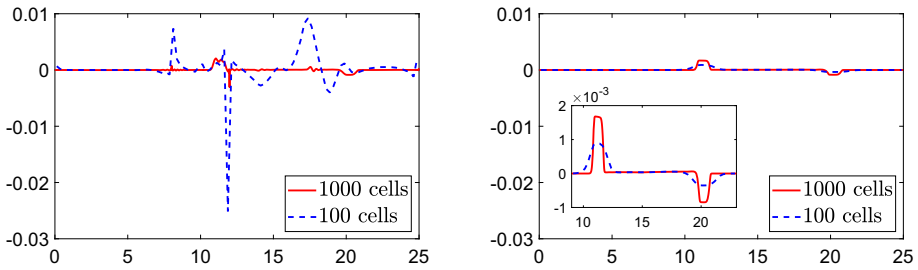


**Fig. 7** Example 5, Case (a): The difference between  $h$  and the background moving steady-state water depth for the Old (left) and New (right) Schemes using 100 (dashed line) and 1000 (solid line) cells

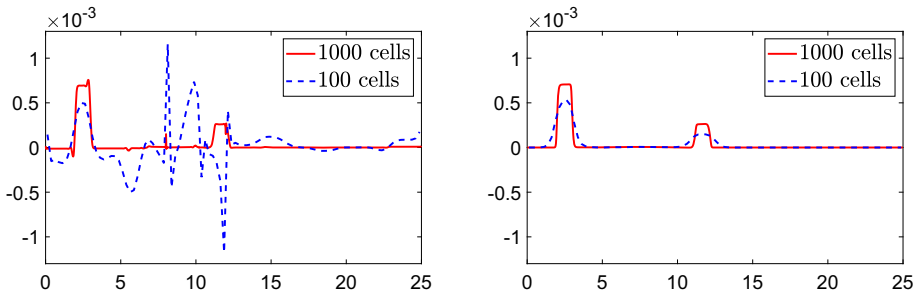


**Fig. 8** Example 5, Case (b): The difference between  $h$  and the background moving steady-state water depth for the Old (left) and New (right) Schemes using 100 (dashed line) and 1000 (solid line) cells

$$B(x) = \begin{cases} 0.2, & \text{if } 8 \leq x \leq 12, \\ 0, & \text{otherwise.} \end{cases} \tag{3.7}$$

We take the same initial and boundary conditions as in Example 4, Cases (a)–(c). In Figs. 9, 10 and 11, we compare the numerical solutions obtained by the New and Old Schemes on a uniform mesh with 100 cells at  $t = 500$ . As one can see, in Cases (a) and (b), quality of the results obtained by both schemes is practically not affected by the presence of the discontinuity in  $B$ . In the transcritical Case (c), the presence of discontinuities in the bottom topography leads to a larger (compared to Example 4) gap between the solutions computed by the New and Old Schemes as the obtained boundary values of  $w$  on the left edge of the computational domain are different. This is attributed to the fact that in this case, the solution is discontinuous and the studied Saint-Venant system (1.1) contains nonconservative product terms, which should be discretized in an extremely careful manner. One of the proper ways of treating such terms is by implementing the path-conservative central-upwind schemes developed in [8], but this is beyond the scope of the current paper.

**Example 7 Small Perturbations of Moving-Water Equilibria (Discontinuous Bottom Topography).** In this example, we test the ability of the New and Old Schemes to capture small perturbations of the moving-water equilibria in the case of discontinuous bottom topography given by (3.7). As in Example 5, we consider the two sets of the steady-state data:

(a) *Supercritical flow with*

$$q(x, 0) \equiv 24, \quad K(x, 0) \equiv 307.624,$$

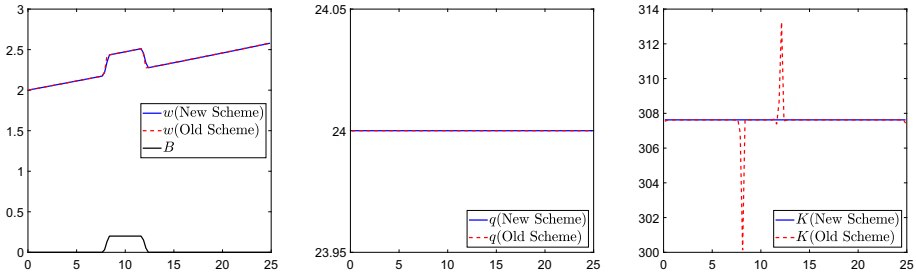


Fig. 9 Example 6, Case (a):  $w$ ,  $q$  and  $K$  (from left to right) computed by the New and Old Schemes

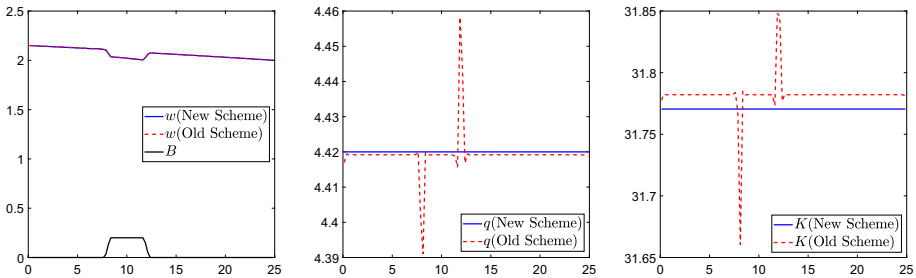


Fig. 10 Example 6, Case (b):  $w$ ,  $q$  and  $K$  (from left to right) computed by the New and Old Schemes

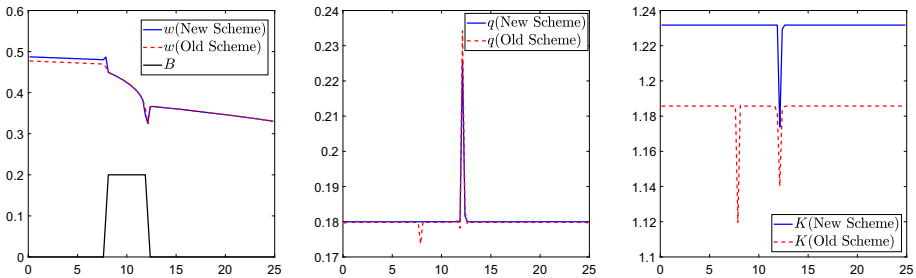


Fig. 11 Example 6, Case (c):  $w$ ,  $q$  and  $K$  (from left to right) computed by the New and Old Schemes

(b) Subcritical flow with

$$q(x, 0) \equiv 4.42, \quad K(x, 0) \equiv 31.7705,$$

and add 0.001 for  $x \in [4.5, 5.5]$  to the corresponding water depth. We compute the solutions until the final time  $t = 1$  using either 100 or 1000 uniform grid cells. The obtained results, reported in Figs. 12 and 13, clearly demonstrate that in the case of discontinuous  $B$ , the New Scheme still captures small perturbations of the moving-water steady state much more accurately than the Old Scheme.

**Example 8 Riemann Problem.** In this example, we test the positivity-preserving property of the New Scheme. We modify the initial data of Example 4, Case (a) to

$$h(x, 0) = \begin{cases} 2, & \text{if } x < 5, \\ 0, & \text{otherwise,} \end{cases} \quad q(x, 0) = \begin{cases} 24, & \text{if } x < 5, \\ 0, & \text{otherwise,} \end{cases}$$

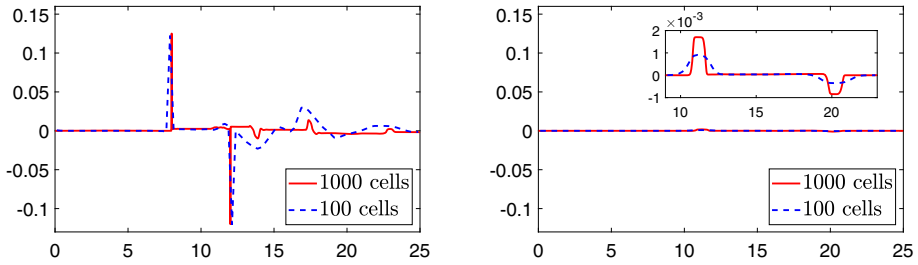


**Fig. 12** Example 7, Case (a): The difference between  $h$  and the background moving steady-state water depth for the Old (left) and New (right) Schemes using 100 (dashed line) and 1000 (solid line) cells

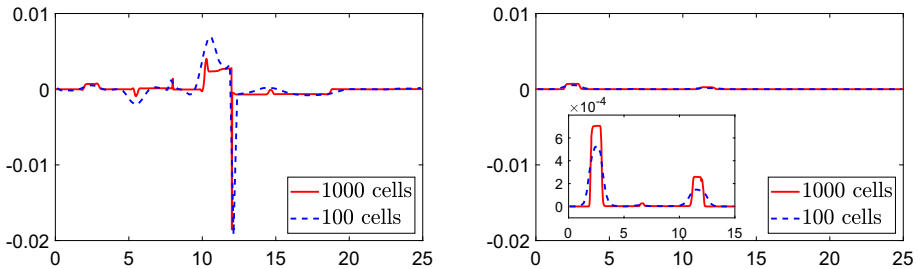


**Fig. 13** Example 7, Case (b): The difference between  $h$  and the background moving steady-state water depth for the Old (left) and New (right) Schemes using 100 (dashed line) and 1000 (solid line) cells

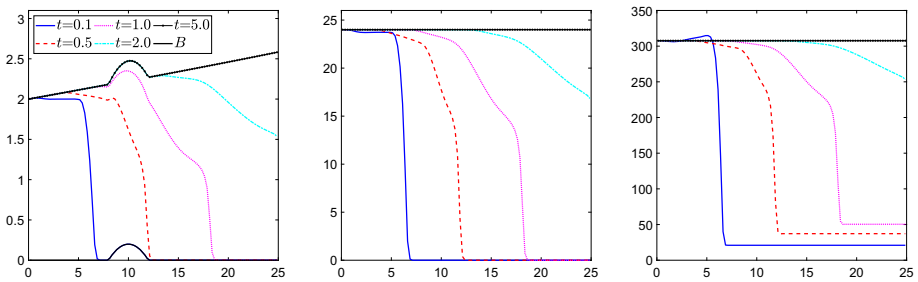


**Fig. 14** Example 8:  $w$ ,  $q$  and  $K$  (from left to right) computed by the New Scheme

and take the same bottom topography and boundary conditions as in Example 4, Case (a). We compute the solutions using 100 uniform grid cells. Figure 14 shows the results at times  $t = 0.1, 0.5, 1, 2$  and  $5$ . As one can clearly see, the water flow runs through the bump and by  $t = 5$  it reaches the same steady state as in Example 4, Case (a) as expected.

**Acknowledgements** The work of A. Chertock was supported in part by NSF Grants DMS-1521051 and DMS-1818684. The work of Y. Cheng was supported in part by NSF Grant DMS-1521009. The work of A. Kurganov was supported in part by NSFC Grant 11771201 and NSF Grant DMS-1521009. The work of M. Herty was supported in part by DFG HE5386/13-15, the cluster of excellence DFG EXC128 “Integrative Production Technology for High-Wage Countries” and the BMBF project KinOpt.

## References

1. Audusse, E., Bouchut, F., Bristeau, M.-O., Klein, R., Perthame, B.: A fast and stable well-balanced scheme with hydrostatic reconstruction for shallow water flows. *SIAM J. Sci. Comput.* **25**, 2050–2065 (2004)
2. Berthon, C., Marche, F., Turpault, R.: An efficient scheme on wet/dry transitions for shallow water equations with friction. *Comput. Fluids* **48**, 192–201 (2011)
3. Bollermann, A., Chen, G., Kurganov, A., Noelle, S.: A well-balanced reconstruction for wet/dry fronts for the shallow water equations. *J. Sci. Comput.* **56**, 267–290 (2013)
4. Bollermann, A., Noelle, S., Lukáčová-Medvid'ová, M.: Finite volume evolution Galerkin methods for the shallow water equations with dry beds. *Commun. Comput. Phys.* **10**, 371–404 (2011)
5. Bouchut, F., Morales, T.: A subsonic well-balanced reconstruction scheme for shallow water flows. *SIAM J. Numer. Anal.* **48**, 1733–1758 (2010)
6. Bryson, S., Epshteyn, Y., Kurganov, A., Petrova, G.: Well-balanced positivity preserving central-upwind scheme on triangular grids for the Saint-Venant system. *M2AN Math. Model. Numer. Anal.* **45**, 423–446 (2011)
7. Castro, M.J., López-García, J.A., Parés, C.: High order exactly well-balanced numerical methods for shallow water systems. *J. Comput. Phys.* **246**, 242–264 (2013)
8. Castro Díaz, M. J., Kurganov, A., Morales de Luna, T.: Path-conservative central-upwind schemes for nonconservative hyperbolic systems. *ESAIM Math. Model. Numer. Anal.* To appear
9. Cea, L., Vázquez-Cendón, M.E.: Unstructured finite volume discretisation of bed friction and convective flux in solute transport models linked to the shallow water equations. *J. Comput. Phys.* **231**, 3317–3339 (2012)
10. Cheng, Y., Kurganov, A.: Moving-water equilibria preserving central-upwind schemes for the shallow water equations. *Commun. Math. Sci.* **14**, 1643–1663 (2016)
11. Chertock, A., Cui, S., Kurganov, A., Özcan, Ş.N., Tadmor, E.: Well-balanced schemes for the Euler equations with gravitation: conservative formulation using global fluxes. *J. Comput. Phys.* **358**, 36–52 (2018)
12. Chertock, A., Cui, S., Kurganov, A., Tong, W.: Steady state and sign preserving semi-implicit Runge–Kutta methods for ODEs with stiff damping term. *SIAM J. Numer. Anal.* **53**, 1987–2008 (2015)
13. Chertock, A., Cui, S., Kurganov, A., Wu, T.: Well-balanced positivity preserving central-upwind scheme for the shallow water system with friction terms. *Int. J. Numer. Meth. Fluids* **78**, 355–383 (2015)
14. Chertock, A., Dudzinski, M., Kurganov, A., Lukáčová-Medvid'ová, M.: Well-balanced schemes for the shallow water equations with Coriolis forces. *Numer. Math.* **138**, 939–973 (2018)
15. Chertock, A., Herty, M., Özcan, Ş. N.: Well-balanced central-upwind schemes for  $2 \times 2$  systems of balance laws. In: Klingenberg, C., Westdickenberg, M. (eds.) *Theory, Numerics and Applications of Hyperbolic Problems I*, vol. 236 of Springer Proceedings in Mathematics and Statistics, Springer International Publishing, pp. 345–361 (2018)
16. de Saint-Venant, A.: *Théorie du mouvement non-permanent des eaux, avec application aux crues des rivières et à l'introduction des marées dans leur lit*, C.R. Acad. Sci. Paris, vol. 73, pp. 147–154 (1871)
17. Gallardo, J., Parés, C., Castro, M.: On a well-balanced high-order finite volume scheme for shallow water equations with topography and dry areas. *J. Comput. Phys.* **227**, 574–601 (2007)
18. Gosse, L.: A well-balanced flux-vector splitting scheme designed for hyperbolic systems of conservation laws with source terms. *Comput. Math. Appl.* **39**, 135–159 (2000)
19. Goutal, N., Maurel, F.: Proceedings of the second workshop on dam-break wave simulation, tech. report, Technical Report HE-43/97/016/A, Electricité de France, Département Laboratoire National d'Hydraulique, Groupe Hydraulique Fluviale, (1997)
20. Jin, S., Wen, X.: Two interface-type numerical methods for computing hyperbolic systems with geometrical source terms having concentrations. *SIAM J. Sci. Comput.* **26**, 2079–2101 (2005)
21. Khan, A., Lai, W.: *Modeling Shallow Water Flows Using the Discontinuous Galerkin Method*. CRC Press, Boca Raton (2014)
22. Kurganov, A.: Finite-volume schemes for shallow-water equations. *Acta Numer.* **27**, 289–351 (2018)
23. Kurganov, A., Levy, D.: Central-upwind schemes for the Saint-Venant system. *M2AN Math. Model. Numer. Anal.* **36**, 397–425 (2002)
24. Kurganov, A., Lin, C.-T.: On the reduction of numerical dissipation in central-upwind schemes. *Commun. Comput. Phys.* **2**, 141–163 (2007)
25. Kurganov, A., Noelle, S., Petrova, G.: Semi-discrete central-upwind scheme for hyperbolic conservation laws and Hamilton–Jacobi equations. *SIAM J. Sci. Comput.* **23**, 707–740 (2001)
26. Kurganov, A., Petrova, G.: A second-order well-balanced positivity preserving central-upwind scheme for the Saint-Venant system. *Commun. Math. Sci.* **5**, 133–160 (2007)

27. Kurganov, A., Polizzi, A.: Non-oscillatory central schemes for a traffic flow model with Arrhenius look-ahead dynamics. *Netw. Heterog. Media* **4**, 416–451 (2009)
28. Kurganov, A., Prugger, M., Wu, T.: Second-order fully discrete central-upwind scheme for two-dimensional hyperbolic systems of conservation laws. *SIAM J. Sci. Comput.* **39**, A947–A965 (2017)
29. Kurganov, A., Tadmor, E.: New high resolution central schemes for nonlinear conservation laws and convection-diffusion equations. *J. Comput. Phys.* **160**, 241–282 (2000)
30. Kurganov, A., Tadmor, E.: Solution of two-dimensional riemann problems for gas dynamics without riemann problem solvers. *Numer. Methods Partial Differ. Equ.* **18**, 584–608 (2002)
31. LeVeque, R.: Balancing source terms and flux gradients in high-resolution Godunov methods: the quasi-steady wave-propagation algorithm. *J. Comput. Phys.* **146**, 346–365 (1998)
32. Nessyahu, H., Tadmor, E.: Nonoscillatory central differencing for hyperbolic conservation laws. *J. Comput. Phys.* **87**, 408–463 (1990)
33. Noelle, S., Xing, Y., Shu, C.-W.: High-order well-balanced finite volume WENO schemes for shallow water equation with moving water. *J. Comput. Phys.* **226**, 29–58 (2007)
34. Perthame, B., Simeoni, C.: A kinetic scheme for the Saint-Venant system with a source term. *Calcolo* **38**, 201–231 (2001)
35. Ricchiuto, M., Bollermann, A.: Stabilized residual distribution for shallow water simulations. *J. Comput. Phys.* **228**, 1071–1115 (2009)
36. Russo, G.: Central schemes for conservation laws with application to shallow water equations. In: *Trends and Applications of Mathematics to Mechanics*. Springer Milan, pp. 225–246 (2005)
37. Russo, G., Khe, A.: High order well balanced schemes for systems of balance laws. In: *Hyperbolic Problems: Theory, Numerics and Applications*, vol. 67 of *Proceedings of Symposium*. Applied Mathematics, American Mathematical Society, Providence, RI, pp. 919–928 (2009)
38. Sweby, P.K.: High resolution schemes using flux limiters for hyperbolic conservation laws. *SIAM J. Numer. Anal.* **21**, 995–1011 (1984)
39. van Leer, B.: Towards the ultimate conservative difference scheme. V. A second-order sequel to Godunov’s method. *J. Comput. Phys.* **32**, 101–136 (1979)
40. Vazquez-Cendon, M.: Improved treatment of source terms in upwind schemes for the shallow water equations in channels with irregular geometry. *J. Comput. Phys.* **148**, 497–526 (1999)
41. Xing, Y.: Exactly well-balanced discontinuous Galerkin methods for the shallow water equations with moving water equilibrium. *J. Comput. Phys.* **257**, 536–553 (2014)
42. Xing, Y., Shu, C.-W.: A survey of high order schemes for the shallow water equations. *J. Math. Study* **47**, 221–249 (2014)
43. Xing, Y., Shu, C.-W., Noelle, S.: On the advantage of well-balanced schemes for moving-water equilibria of the shallow water equations. *J. Sci. Comput.* **48**, 339–349 (2011)

**Publisher’s Note** Springer Nature remains neutral with regard to jurisdictional claims in published maps and institutional affiliations.